Progress of Theoretical Physics, Vol. 106, No. 1, July 2001

Universal Bicritical Behavior of Period Doublings in Unidirectionally Coupled Oscillators

Sang-Yoon KIM,[1,*)] Woochang LIM[1] and Youngtae KIM[2]

[1]*Department of Physics, Kangwon National University, Chunchon Kangwon-Do 200-701, Korea*
[2]*Department of Molecular Science and Technology, Ajou University, Suwon Kyunggi-Do 442-749, Korea*

(Received March 1, 2001)

We study the bicritical behavior of period doublings in unidirectionally coupled oscillators to confirm the universality of the bicriticality in an abstract system of two unidirectionally coupled one-dimensional (1D) maps. A transition to hyperchaos occurs (i.e., a hyperchaotic attractor with two positive Lyapunov exponents appears) when crossing a bicritical point where two Feigenbaum critical lines of a period-doubling transition to chaos in the two subsystems meet. Using both a "residue-matching" renormalization group method and a direct numerical method, we make an analysis of the scaling behavior near the bicritical point. It is thus found that the second response subsystem exhibits a new type of non-Feigenbaum critical behavior, while the first drive subsystem is in the usual Feigenbaum critical state. Note that the bicritical scaling behavior is the same as that in the unidirectionally coupled 1D maps. We thus suppose that bicriticality may be observed generally in real systems, consisting of period-doubling subsystems with a unidirectional coupling.

§1. Introduction

Period-doubling transitions to chaos have been extensively studied in a one-parameter family of 1D unimodal maps. As the control parameter is varied, the 1D map undergoes a period-doubling cascade, leading to chaos. Feigenbaum has developed a renormalization group (RG) method, and discovered universal scaling behavior near the accumulation point of such a period-doubling cascade.[1)] The universality of the Feigenbaum criticality has been confirmed in a large number of real physical systems and ordinary differential equations.[2)] For example, nonlinear oscillators such as the forced Duffing oscillator[3)] and the Rössler oscillator[4)] belong to the Feigenbaum universality class.

Recently, great effort has been made in studies of coupled systems, consisting of period-doubling subsystems, in an attempt to generalize the study of this type to high-dimensional nonlinear systems.[3)-9)] Here we are interested in bicritical scaling behavior of period doublings in unidirectionally coupled systems. These unidirectionally coupled systems are usually used as models for open flow systems.[10)] A new kind of non-Feigenbaum scaling behavior has been found in an abstract system of two unidirectionally coupled 1D maps near a bicritical point where two Feigenbaum critical lines of a period-doubling transition to chaos in the two subsystems meet.[7),8)] In this paper we study the bicritical scaling behavior of period doublings

*) E-mail: sykim@cc.kangwon.ac.kr

in unidirectionally coupled oscillators to confirm the universality of the bicriticality in an abstract system of two unidirectionally coupled 1D maps.

One of the representative nonlinear oscillators that undergoes period-doubling cascades is the forced double-well Duffing oscillator (DWDO).[11] In this paper we investigate a system consisting of two forced DWDOs with unidirectional coupling. For this unidirectionally coupled system, the drive subsystem acts on the response subsystem, but the response subsystem does not influence the drive subsystem. Hence the two unidirectionally coupled DWDOs have a skew product structure.[12] For a single forced DWDO, when the forcing amplitude A is increased, the asymmetric periodic orbits arising from the two stable equilibrium points of the double-well potential exhibit period-doubling cascades, leading to chaos, as in the 1D map.[1] However, as A is increased further, reversals of period-doubling cascades occur, in contrast to the monotone behavior of the 1D map. Hereafter, the former cascade, creating periodic orbits, will be called the "forward cascade", while the latter one, destroying periodic orbits, will be called the "backward cascade". The types of scaling behavior at accumulation points of both the forward and backward cascades are the same as those for the 1D map case. Note also that this kind of antimonotone behavior of the concurrent creation and destruction of periodic orbits has been observed in many other physical systems.[13]

Here we follow the sequence of period doublings in two unidirectionally coupled DWDOs by varying the two control parameters A and B of the two subsystems for a fixed value of the coupling parameter C. Scaling behavior is thus investigated near a bicritical point (A_c, B_c), where two Feigenbaum critical lines of period-doubling transitions to chaos in the two subsystems meet. Note that this bicritical point corresponds to the border of chaos in both subsystems. Hence, when crossing such a bicritical point, a hyperchaotic attractor with two positive Lyapunov exponents[14] appears; i.e., a transition to hyperchaos occurs. Varying A or B, each subsystem in the unidirectionally coupled DWDOs may undergo forward and backward period-doubling cascades, leading to chaos. As a result of this antimonotone behavior, four bicritical points exist in the A-B plane, in contrast to the unidirectionally coupled 1D maps exhibiting monotone behavior.[7),8)] Employing both a RG method and a direct numerical method, we investigate the scaling behavior near each bicritical point, and find that the response subsystem exhibits a new kind of non-Feigenbaum scaling behavior, while the drive subsystem is in the usual Feigenbaum critical state. Note that this bicritical scaling behavior is the same as that in an abstract system of two unidirectionally coupled 1D maps.[7),8)] Furthermore, to examine the universality of such bicriticality, we also investigate another unidirectionally coupled system, consisting of two autonomous Rössler oscillators,[15] and find the same bicritical scaling behavior. Hence, we suppose that such bicriticality is a generic phenomenon, occurring in many real systems consisting of period-doubling subsystems.

This paper is organized as follows. We first introduce two unidirectionally coupled DWDOs in §2, and then discuss the stability and bifurcations of periodic orbits. In particular, a convenient real quantity, called the "residue",[16] is used to characterize the stability of periodic orbits and their bifurcations. In §3, using both a residue-matching RG method and a direct numerical method, we investigate scaling

behavior near the bicritical points, and find non-Feigenbaum scaling behavior in the second response subsystem. Note that this bicritical behavior is the same as that in two unidirectionally coupled 1D maps. To examine the universality of the bicriticality, unidirectionally coupled Rössler oscillators are also investigated. Finally, a summary is given in §4.

§2. Stability and bifurcations of periodic orbits

In this section, we first discuss the stability of period orbits in the four-dimensional (4D) Poincaré map of the two unidirectionally coupled DWDOs, using the Floquet theory.[17] Bifurcations associated with the stability and Lyapunov exponents are then discussed.

A single DWDO can be described by two first-order ordinary differential equations,[18]

$$\dot{x} = y, \tag{1a}$$
$$\dot{y} = f_A(x, y, t), \tag{1b}$$

where $f_A(x, y, t) = -\gamma y + x - x^3 + A\cos\omega t$, γ is the damping coefficient, $A\cos\omega t$ is a driving force with amplitude A and frequency ω, and the overdot denotes differentiation with respect to time t. Two identical DWDOs are then coupled together with a unidirectional coupling type:

$$\dot{x}_1 = y_1, \tag{2a}$$
$$\dot{y}_1 = f_A(x_1, y_1, t), \tag{2b}$$
$$\dot{x}_2 = y_2 + C(x_2 - x_1), \tag{2c}$$
$$\dot{y}_2 = f_B(x_2, y_2, t) + C(y_2 - y_1). \tag{2d}$$

Here, A and B are the driving amplitudes of the external driving forces of the two DWDOs and C is a coupling parameter. For this unidirectionally coupled system, the first master DWDO with state variables x_1 and y_1 can be regarded as a driving equation for the second slave or response DWDO with state variables x_2 and y_2 through the coupling term. These unidirectionally coupled DWDOs are symmetric with respect to the transformation S, defined as

$$S : x_1 \to -x_1,\ y_1 \to -y_1,\ x_2 \to -x_2,\ y_2 \to -y_2,$$
$$t \to t + \frac{T}{2} \quad \left[T(\text{period}) = \frac{2\pi}{\omega}\right], \tag{3}$$

as this leaves Eq. (2d) invariant. If an orbit $\boldsymbol{z}(t)[\equiv (z_1(t), z_2(t))]$, where $z_i = (x_i, y_i)$ $(i = 1, 2)$, is invariant under S, then it is called a symmetric orbit. Otherwise, it is called an asymmetric orbit and has its conjugate orbit $S\boldsymbol{z}(t)$.

The phase space of the two unidirectionally coupled DWDOs is five dimensional, with coordinates x_1, y_1, x_2, y_2, and t. Since the unidirectionally coupled DWDOs are periodic in t, it is convenient to regard time as a circular coordinate (with mod T) in the phase space. We then consider the surface of a section, the x_1-y_1-x_2-y_2

hypersurface, at times $t = mT$ (m: integer). The phase space trajectory intersects this hypersurface in a sequence of points. This sequence of points corresponds to a mapping on the 4D hypersurface. This map plot of an initial orbit point $\boldsymbol{z}(0)$ can be computed by stroboscopically sampling the orbit points $\boldsymbol{z}(m)$ at the discrete time mT. We call the transformation $\boldsymbol{z}(m) \to \boldsymbol{z}(m+1)$ the Poincaré map, and write $\boldsymbol{z}(m+1) = P(\boldsymbol{z}(m))$. This 4D Poincaré map (symmetric with respect to S) may have many attractors for fixed parameter values. For $A = B$ and $C = 0$, it breaks up into two uncoupled identical two-dimensional (2D) maps possessing symmetry with respect to S. If each uncoupled 2D map has either an asymmetric stable orbit z [$= (x, y)$] or its conjugate orbit z^*, then the composite 4D map has one of the four pairs of orbits (z, z), (z^*, z^*), (z, z^*), and (z^*, z). For the first and second (third and fourth) pairs, the 2D uncoupled maps have the same (different) kind of orbits. Hereafter, the corresponding pairs will be called the "same (different) pairs". To classify the orbits in the composite 4D map, we should also take the phase shift between the uncoupled 2D maps into consideration. If each 2D map has a stable orbit of period 2^n, then the composite 4D map has 2^n different states distinguished by the phase shift N ($N = 0, \cdots, 2^n - 1$). Note that this multistability is preserved when the coupling is introduced, at least while its value is sufficiently small. Hereafter, an orbit will be called an orbit of type $N_{s(d)}$ if it corresponds to the same (different) pair and there exists a phase shift N between the state variables z_1 and z_2 of the first and second 2D maps [i.e., $z_1(m) = z_2(m+N)$] when we come to the point $C = 0$ and $A = B$.

The linear stability of a q-periodic orbit of the 4D Poincaré map P, such that $P^q(\boldsymbol{z}(0)) = \boldsymbol{z}(0)$, is determined from the linearized-map matrix M [$\equiv DP^q(\boldsymbol{z}(0))$] of P^q at an orbit point $\boldsymbol{z}(0)$. Here P^q represents the q-times iterated map. Using the Floquet theory,[17] the matrix M can be obtained by integrating the linearized differential equations for small perturbations with four initial perturbations, $(\delta x_1, \delta y_1, \delta x_2, \delta y_2) = (1,0,0,0)$, $(0,1,0,0)$, $(0,0,1,0)$, and $(0,0,0,1)$ over the period q. Since an unidirectionally coupled system has a skew product structure,[12] the linearized-map matrix M has the semiblock form

$$M = \begin{pmatrix} M_1 & \mathbf{0} \\ M_3 & M_2 \end{pmatrix}, \tag{4}$$

where $\mathbf{0}$ is the 2×2 null matrix. Hence, in order to determine the eigenvalues of M, it is sufficient to solve the eigenvalue problems of the two 2×2 submatrices M_1 and M_2, independently. Here $M_1(A)$ and $M_2(B, C)$ determine the stability of the drive and response subsystems, respectively. Note also that the first submatrix M_1 is just the linearized Poincaré map of the DWDO,[18] and the coupling affects only the second submatrix M_2.

The eigenvalues $\lambda_{i,1}$ and $\lambda_{i,2}$ of M_i ($i = 1, 2$) are called the Floquet (stability) multipliers. They characterize the stability of the ith subsystem. Note also that the first pair of Floquet multipliers, $(\lambda_{1,1}, \lambda_{1,2})$, is just the pair of Floquet multipliers of the uncoupled DWDO,[18] and the coupling affects only the second pair of Floquet multipliers, $(\lambda_{2,1}, \lambda_{2,2})$. By using the Liouville formula,[19] we obtain constant

Jacobian determinants $\mathcal{D}_1$ and $\mathcal{D}_2$ of the submatrices M_1 and M_2, respectively, where

$$\mathcal{D}_1 = e^{-\gamma q}, \quad \mathcal{D}_2 = e^{-(\gamma - 2C)q}. \tag{5}$$

Hence the ith pair of Floquet multipliers lies either on the circle of radius $\sqrt{D_i}$ or on the real axis in the complex plane. A periodic orbit becomes stable when all its four Floquet multipliers lie inside the unit circle in the complex plane (i.e., their moduli are less than unity). Here we consider the case of $\mathcal{D}_i < 1$; $\mathcal{D}_1$ is always less than unity, while $\mathcal{D}_2$ becomes less than unity for $C < \gamma/2$. Then, the two pairs of Floquet multipliers never cross the unit circle in the complex plane, except at the real axis, and hence Hopf bifurcations do not occur. Consequently, a stable periodic orbit can lose its stability only when a Floquet multiplier λ_i passes through 1 or -1 on the real axis.

A more convenient real quantity $\mathcal{R}_i$ $(i = 1, 2)$, called the residue [16] and defined by

$$\mathcal{R}_i \equiv \frac{1 + \mathcal{D}_i - \mathcal{T}_i}{2(1 + \mathcal{D}_i)}, \tag{6}$$

is used to characterize the stability of periodic oscillations in the ith subsystem. Here $\mathcal{D}_i$ and $\mathcal{T}_i$ are the determinant and trace of the submatrix M_i, respectively. Then the Floquet multipliers λ_i can be expressed in terms of $\mathcal{R}_i$ as follows:

$$\lambda_i = \frac{(1 + \mathcal{D}_i)}{2}\left(1 - 2\mathcal{R}_i \pm 2\sqrt{(\mathcal{R}_i - \mathcal{R}^*_{i,1})(\mathcal{R}_i - \mathcal{R}^*_{i,2})} \right), \tag{7}$$

where

$$\mathcal{R}^*_{i,1} = \frac{(1 - \sqrt{\mathcal{D}_i})^2}{2(1 + \mathcal{D}_i)}, \quad \mathcal{R}^*_{i,2} = \frac{(1 + \sqrt{\mathcal{D}_i})^2}{2(1 + \mathcal{D}_i)}. \tag{8}$$

For $\mathcal{R}^*_{i,1} < \mathcal{R}_i < \mathcal{R}^*_{i,2}$, Floquet multipliers occur in complex-conjugate pairs (λ_i, λ_i^*) on the circle of radius $\sqrt{\mathcal{D}_i}$, while they come in real pairs $(\lambda_i, \mathcal{D}_i/\lambda_i)$ on the real axis for $\mathcal{R}_i < \mathcal{R}^*_{i,1}$ or $\mathcal{R} > \mathcal{R}^*_{i,2}$. Note also that the Floquet multipliers can cross the unit circle only at the real axis (i.e., at $\lambda_i = 1$ or -1). For $\lambda_i = 1$ and -1, the values of $\mathcal{R}_i$ are 0 and 1, respectively. Hence, when $0 < \mathcal{R}_i < 1$, the pair of Floquet multipliers λ_i lies inside the unit circle. As R_i decreases through 0 (i.e., a Floquet multiplier λ_i increases through 1), the periodic orbit loses its stability via a saddle-node or pitchfork bifurcation. Contrastingly, as $\mathcal{R}_i$ increases through 1 (i.e., a Floquet multiplier decreases through -1), it becomes unstable via a period-doubling bifurcation. (For more detailed discussion of bifurcations, refer to Ref. 21).)

Finally, we briefly discuss Lyapunov exponents [22] of an orbit in the 4D Poincaré map P. The two submatrices M_1 and M_2 of M determine the Lyapunov exponents $(\sigma_{1,1}, \sigma_{1,2})$ and $(\sigma_{2,1}, \sigma_{2,2})$, characterizing the average exponential rates of divergence of nearby orbits in the first and second subsystems, respectively, where $\sigma_{i,1} \geq \sigma_{i,2}$ for $i = 1, 2$. Since the two submatrices have the constant Jacobian determinants given in Eq. (5), the two pairs of Lyapunov exponents satisfy $\sigma_{1,1} + \sigma_{1,2} = -2\gamma$ and $\sigma_{2,1} + \sigma_{2,2} = -\gamma + 2C$. Note also that the first pair of Lyapunov exponents, $(\sigma_{1,1}, \sigma_{1,2})$, is just the pair of Lyapunov exponents of the uncoupled DWDO, [18] and the coupling affects only the second pair of Lyapunov exponents, $(\sigma_{2,1}, \sigma_{2,2})$.

§3. Universal bicritical behavior of period doublings

In this section, by varying the two control parameters A and B of the two subsystems for a fixed value of the coupling parameter C, we study the bicritical scaling behavior in the two unidirectionally coupled DWDOs with $\gamma = 0.2$ and $\omega = 2.8$. When crossing a bicritical point, corresponding to a border of chaos in both subsystems, a transition to hyperchaos occurs; i.e., a hyperchaotic attractor with two positive Lyapunov exponents appears. Varying a control parameter A or B, each subsystem in the unidirectionally coupled DWDOs may undergo forward and backward period-doubling cascades. As a consequence of this antimonotone behavior, four bicritical points exist in the A-B plane, in contrast with the unidirectionally coupled 1D maps exhibiting monotone behavior. Using both the residue-matching RG method and a direct numerical method, we investigate various scaling behavior near each bicritical point. A new type of non-Feigenbaum scaling behavior is thereby found in the second response subsystem. To examine the universality of the bicriticality, we also study two unidirectionally coupled Rössler oscillators. Note that this bicritical scaling behavior in unidirectionally coupled oscillators is the same as that in an abstract system of unidirectionally coupled 1D maps.[7),8)]

We now fix the coupling parameter as $C = -0.1$ and study period-doubling bifurcations by increasing B from zero. Hence the periodic orbits that exist from $B = 0$ become the "mother" orbits for such period-doubling cascades. These mother orbits are orbits of type "0_s", because they are in-phase (phase-shift $N = 0$) and consist of the same pairs when coming to $A = B$ and $C = 0$ (refer to §2 for type of orbits).

As in the case of the uncoupled DWDO,[18)] when A is increased, the asymmetric fixed points of the Poincaré map P, arising from the stable equilibrium points ($x = \pm 1$) of the double-well potential, exhibit period-doubling cascades, leading to chaos, in the first subsystem. However, as A is further increased, reversals of period-doubling cascades occur. This kind of antimonotone behavior of the concurrent creation and destruction of periodic orbits contrasts with the monotone behavior of the 1D map.[1)] The forward cascade, creating periodic orbits, and the backward cascade, destroying periodic orbits, in the first subsystem are shown in Fig. 1(a). Similarly, as B is increased, for a fixed A, the second subsystem also exhibits antimonotone behavior, as shown in Fig. 1(b).

Figure 2 displays stability diagrams of asymmetric periodic orbits. Each stable region is labelled by a pair of numbers, (q_1, q_2), where q_1 and q_2 are the periods of oscillations in the first and second subsystems, respectively. The first subsystem exhibits a forward period-doubling cascade, creating periodic orbits, at the vertical straight lines, where $R_1 = 1$. These period doublings accumulate at a critical line, denoted by the vertical dashed line located at $A = A_\infty^{\rm F}$ ($= 1.834\,473\,233$). However, as A is further increased, a backward period-doubling cascade, destroying periodic orbits, also occurs in the first subsystem at the vertical straight lines, where $R_1 = 1$. These period doublings accumulate at another critical line, denoted also by a vertical dashed line and located at $A = A_\infty^{\rm B}$ ($= 4.245\,906\,614$). When crossing a vertical dashed critical line, a transition to chaos occurs in the first subsystem. For

small values of the parameter B, the second subsystem exhibits a forced response whose period is the same as that of the first subsystem. As B is increased for a fixed value of A, the second subsystem also undergoes forward and backward period-doubling cascades at the non-vertical solid lines, where $R_2 = 1$, accumulating at the critical lines denoted by non-vertical dashed lines. When crossing a non-vertical critical line, a transition to chaos takes place in the second subsystem. Note that the vertical and non-vertical critical lines meet at four bicritical points, denoted by solid circles, corresponding to the threshold of chaos in both subsystems. Consequently, when crossing a bicritical point, a hyperchaotic attractor with two positive Lyapunov exponents appears.

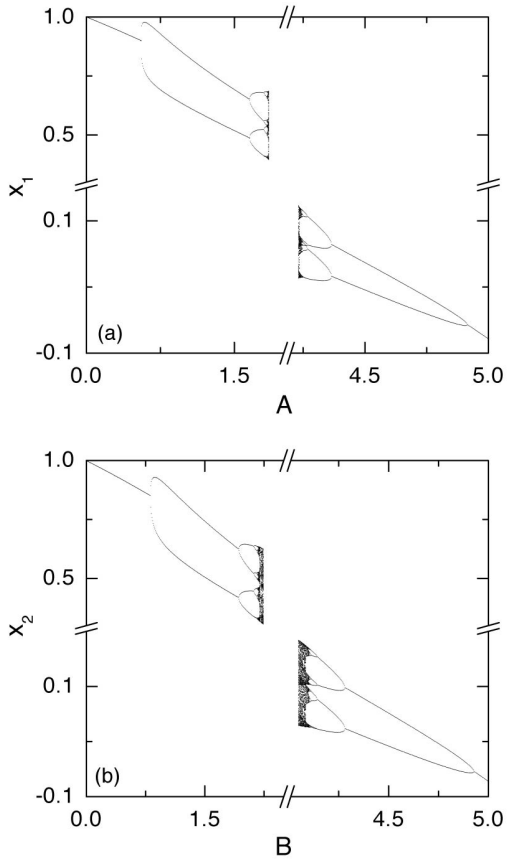

Fig. 1. Antimonotone behavior of the first and second subsystems for $C = -0.1$. (a) The forward and backward period-doubling cascades in the first subsystem. (b) The forward and backward period-doubling cascades in the second subsystem for $A = 0.5$.

To analyze the scaling behavior near the bicritical points, we first develop a residue-matching RG method, equating the residues of the orbit of level n (period 2^n) to those of the orbit of the next level, $n+1$. The basic idea of the residue-matching RG method is to associate a pair of values (A', B') for each (A, B) such that $P^{(n+1)}_{(A',B')}$ locally resembles $P^{(n)}_{(A,B)}$, where $P^{(n)}$ is the 2^nth-iterated map of P (i.e., $P^{(n)} = P^{2^n}$). Here A and B are the control parameters of the two subsystems, and the coupling parameter C is fixed. A simple way to implement this idea is to linearize the maps in the neighborhood of their respective fixed points and equate the corresponding residues, characterizing their stability. This residue-matching RG method can be regarded as a generalized version of the eigenvalue-matching RG method that has been successfully used in the two unidirectionally-coupled 1D maps.[8] Note also that residue matching in slightly different contexts has also been used to study the breakup of invariant circles in area-preserving twist maps.[20]

Consider two successive orbits of period 2^n and 2^{n+1}, $\{\boldsymbol{z}(m)\}$ and $\{\boldsymbol{z}'(m)\}$, such that

$$\boldsymbol{z}(m) = P^{(n)}_{(A,B)}(\boldsymbol{z}(m)),\ \boldsymbol{z}'(m) = P^{(n+1)}_{(A',B')}(\boldsymbol{z}'(m)), \tag{9}$$

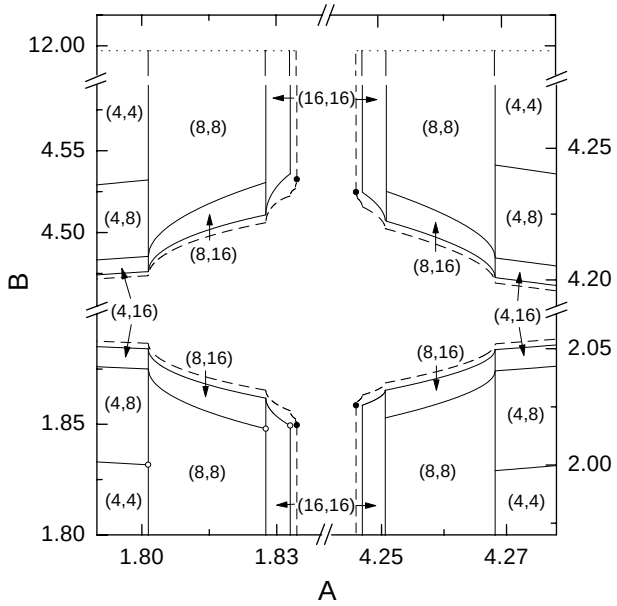

Fig. 2. Stability diagram of asymmetric periodic orbits for $C = -0.1$. Each stable region is labeled by a pair of numbers (q_1, q_2), where q_1 and q_2 are the periods of oscillations in the first and second subsystems, respectively. The vertical (nonvertical) solid lines represent the period-doubling bifurcation lines in the first (second) subsystem, and the uppermost dotted lines denote the saddle-node bifurcation lines in the second subsystem. When crossing the vertical and nonvertical dashed lines, transitions to chaos occur in the first and second subsystems, respectively. Note that these critical lines meet at the four bicritical points, denoted by the solid circles, which correspond to the border of chaos in both subsystems. Furthermore, the open circles denote the points, corresponding to the threshold of instability in both subsystems, where $R_1 = 1$ and $R_2 = 1$. Such open circles also accumulate at the lower-left bicritical point.

where $\boldsymbol{z} = (z_1, z_2)$ and $z_i = (x_i, y_i)$. Here the state variable z_1 of the first subsystem depends only on A, but the state variable z_2 of the second subsystem is dependent on both A and B. Linearizing $P^{(n)}$ and $P^{(n+1)}$ at $\boldsymbol{z}(m)$ and $\boldsymbol{z}'(m)$, respectively, we obtain

$$DP^{(n)}_{(A,B)} = \prod_{m=1}^{2^n} DP_{(A,B)}(\boldsymbol{z}(m)),\ DP^{(n+1)}_{(A',B')} = \prod_{m=1}^{2^{n+1}} DP_{(A',B')}(\boldsymbol{z}'(m)), \tag{10}$$

where DP is the linearized Poincaré map of P. Then the eigenvalues of the linearized-map matrices, called the Floquet multipliers, determine the stability of the periodic orbits. However, as explained in §2, it is more convenient to use the residues $\mathcal{R}_1$ and $\mathcal{R}_2$, defined in Eq. (6), to characterize the stability of periodic oscillations in the first and second subsystems, respectively. The recurrence relations for the old and new parameters are then given by equating the residues of level n, $\mathcal{R}_{1,n}(A)$ and $\mathcal{R}_{2,n}(A, B)$, to those of level $n + 1$, $\mathcal{R}_{1,n+1}(A')$ and $\mathcal{R}_{2,n+1}(A', B')$:

$$\mathcal{R}_{1,n}(A) = \mathcal{R}_{1,n+1}(A'), \tag{11a}$$

$$\mathcal{R}_{2,n}(A, B) = \mathcal{R}_{2,n+1}(A', B'). \tag{11b}$$

The fixed point (A^*, B^*) of the renormalization transformation (11b),

$$\mathcal{R}_{1,n}(A^*) = \mathcal{R}_{1,n+1}(A^*), \tag{12a}$$

$$\mathcal{R}_{2,n}(A^*, B^*) = \mathcal{R}_{2,n+1}(A^*, B^*), \tag{12b}$$

gives the bicritical point (A_c, B_c), corresponding to the border of chaos in both subsystems, for a fixed C. By linearizing the renormalization transformation at the fixed point (A^*, B^*), we obtain

$$\begin{pmatrix} \Delta A \\ \Delta B \end{pmatrix} = \begin{pmatrix} \frac{\partial A}{\partial A'}\Big|_* & \frac{\partial A}{\partial B'}\Big|_* \\ \frac{\partial B}{\partial A'}\Big|_* & \frac{\partial B}{\partial B'}\Big|_* \end{pmatrix} \begin{pmatrix} \Delta A' \\ \Delta B' \end{pmatrix} \tag{13}$$

$$= \Delta_n \begin{pmatrix} \Delta A' \\ \Delta B' \end{pmatrix}, \tag{14}$$

where

$$\Delta_n = \Gamma_n^{-1}\Gamma_{n+1}, \tag{15}$$

$$\Gamma_n = \begin{pmatrix} \frac{d\mathcal{R}_{1,n}}{dA}\Big|_* & 0 \\ \frac{\partial \mathcal{R}_{2,n}}{\partial A}\Big|_* & \frac{\partial \mathcal{R}_{2,n}}{\partial B}\Big|_* \end{pmatrix}, \tag{16}$$

$$\Gamma_{n+1} = \begin{pmatrix} \frac{d\mathcal{R}_{1,n+1}}{dA'}\Big|_* & 0 \\ \frac{\partial \mathcal{R}_{2,n+1}}{\partial A'}\Big|_* & \frac{\partial \mathcal{R}_{2,n+1}}{\partial B'}\Big|_* \end{pmatrix}. \tag{17}$$

Here Γ_n^{-1} is the inverse of Γ_n, and the asterisk denotes the fixed point (A^*, B^*). After some algebra, we obtain analytic formulas for the eigenvalues $\delta_{1,n}$ and $\delta_{2,n}$ of the matrix Δ_n,

$$\delta_{1,n} = \frac{\frac{d\mathcal{R}_{1,n+1}}{dA'}\Big|_*}{\frac{d\mathcal{R}_{1,n}}{dA}\Big|_*}, \tag{18a}$$

$$\delta_{2,n} = \frac{\frac{\partial \mathcal{R}_{2,n+1}}{\partial B'}\Big|_*}{\frac{\partial \mathcal{R}_{2,n}}{\partial B}\Big|_*}. \tag{18b}$$

As $n \to \infty$, the eigenvalues of level n, $\delta_{1,n}$ and $\delta_{2,n}$, approach their limiting values, δ_1 and δ_2, which are just the parameter scaling factors in the first and second subsystems, respectively.

In addition to the parameter scaling factors, we can also obtain the orbital scaling factors. To look for simple scaling in the phase space at the bicritical point (A_n^*, B_n^*) of level n, we first locate the most rarefied region by choosing a 2^n-periodic orbit point $\boldsymbol{z}^{(n)}(0)$ that has the largest distance from its nearest orbit point $\boldsymbol{z}^{(n)}(2^{n-1})$ $[= P^{2^{n-1}}(\boldsymbol{z}^{(n)}(0))]$. Then, the local rescaling factors of the state variables are simply given by

$$\alpha_{x_1,n} = \frac{d_{x_1,n}}{d_{x_1,n+1}}, \quad \alpha_{y_1,n} = \frac{d_{y_1,n}}{d_{y_1,n+1}}, \tag{19a}$$

$$\alpha_{x_2,n} = \frac{d_{x_2,n}}{d_{x_2,n+1}}, \quad \alpha_{y_2,n} = \frac{d_{y_2,n}}{d_{y_2,n+1}}, \tag{19b}$$

where

$$d_{x_1,n} \equiv x_1^{(n)}(0) - x_1^{(n)}(2^{n-1}), \quad d_{y_1,n} \equiv y_1^{(n)}(0) - y_1^{(n)}(2^{n-1}), \tag{20a}$$

$$d_{x_2,n} \equiv x_2^{(n)}(0) - x_2^{(n)}(2^{n-1}), \quad d_{y_2,n} \equiv y_2^{(n)}(0) - y_2^{(n)}(2^{n-1}). \tag{20b}$$

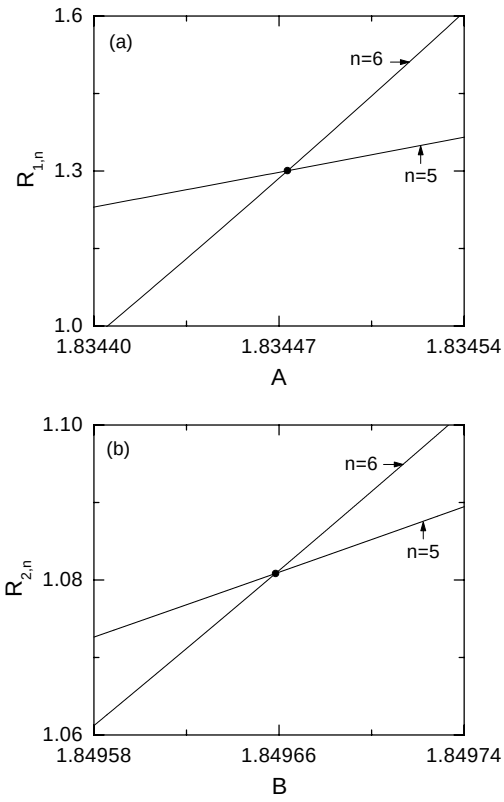

Fig. 3. Plots of (a) the first residue $R_{1,n}(A)$ as a function of A and (b) the second residue $R_{2,n}(A_5^*, B)$ as a function of B for the cases $n = 5, 6$. In (a), the intersection point, denoted by the solid circle, of the two curves $R_{1,5}$ and $R_{1,6}$ gives the point $(A_5^*, R_{1,5}^*)$ of level 5. As $n \to \infty$, $(A_n^*, R_{1,n}^*)$ converges to its limit point, (A^*, R_1^*). Similarly, in (b), the intersection point, denoted also by the solid circle, of the two successive curves $R_{2,5}(A_5^*, B)$ and $R_{2,6}(A_5^*, B)$ gives the point $(B_5^*, R_{2,5}^*)$ of level 5. As $n \to \infty$, $(B_n^*, R_{2,n}^*)$ also approaches its limit point, (B^*, R_2^*).

As $n \to \infty$, both the rescaling factors $\alpha_{x_1,n}$ and $\alpha_{y_1,n}$ of level n converge to the orbital scaling factor α_1 in the first subsystem, while $\alpha_{x_2,n}$ and $\alpha_{y_2,n}$ converge to the orbital scaling factor α_2 in the second subsystem.

Using the above described residue-matching RG method, we make an analysis of the scaling behavior near the lower-left bicritical point (A_c, B_c) $[=(A_\infty^{\rm F}, 1.849\,69)]$, corresponding to the forward-forward period-doubling cascades in the first-second subsystems (see Fig. 2). Figure 3 displays some RG results obtained by matching the residues of intermediate level $n = 5, 6$. Plots of the first residue $\mathcal{R}_{1,n}(A)$ versus A for the cases $n = 5, 6$ are shown in Fig. 3(a). Note that the intersection point, denoted by the solid circle, of the two curves $\mathcal{R}_{1,5}(A)$ and $\mathcal{R}_{1,6}(A)$ gives the point $(A_5^*, \mathcal{R}_{1,5}^*)$, where A_5^* and $\mathcal{R}_{1,5}^*$ are the critical point and critical residue of level 5 in the first subsystem, respectively. As shown in Eq. (18a), the ratio of the slopes of the curves, $\mathcal{R}_{1,5}$ and $\mathcal{R}_{1,6}$, for $A = A_5^*$ gives the parameter scaling factor $\delta_{1,5}$ of level 5 in the first subsystem. Similarly, Fig. 3(b) displays plots of the second residue $\mathcal{R}_{2,n}(A_5^*, B)$ versus B for the cases $n = 5, 6$. The intersection point, denoted also by the solid circle, of the two curves $\mathcal{R}_{2,5}(A_5^*, B)$ and $\mathcal{R}_{2,6}(A_5^*, B)$ gives the point $(B_5^*, \mathcal{R}_{2,5}^*)$, where B_5^* and $\mathcal{R}_{2,5}^*$ are the critical point and critical residue of level 5 in the second subsystem, respectively. As shown in Eq. (18b), the ratio of the slopes of the curves,

$\mathcal{R}_{2,5}(A_5^*, B)$ and $\mathcal{R}_{2,6}(A_5^*, B)$, for $B = B_5^*$ gives the parameter scaling factor $\delta_{2,5}$ of level 5 in the second subsystem. Increasing the level up to $n = 9$, we first solve Eq. (12b) to obtain the bicritical point (A_n^*, B_n^*) of level n and a pair of critical residues $(\mathcal{R}_{1,n}^*, \mathcal{R}_{2,n}^*)$ of level n. Next, using Eqs. (18) and (19b), we obtain the parameter and orbital scaling factors of level n, respectively. Then, as the level n is increased, the sequences of the critical points, critical residues, parameter and orbital scaling factors of level n converge to their limit values.

The RG results for the first drive subsystem are listed in Table I. As n is increased, the sequence of values of the parameter scaling factor $\delta_{1,n}$ converges to the limit value δ_1 ($\simeq 4.669$), and the sequences of values of the orbital scaling factors $\alpha_{x_1,n}$ and $\alpha_{y_1,n}$ approach the same limit value α_1 ($\simeq -2.5$). Note that these limit values δ_1 and α_1 agree well with Feigenbaum constants δ ($= 4.669\cdots$) and α ($= -2.502\cdots$) for 1D maps.[1] When n is increased, the sequence of the critical residue $\mathcal{R}_{1,n}^*$ also converges to the limit value $\mathcal{R}^*$ ($\simeq 1.3$). As shown in Eq. (5), the determinant $\mathcal{D}_1$ of the linearized-map matrix M_1 for the q-periodic ($q = 2^n$) orbit of level n goes to zero as $n \to \infty$. Then, one can easily see from Eq. (7) that the pair of critical Floquet multipliers $(\lambda_{1,1}^*, \lambda_{1,2}^*)$ becomes $(1 - 2R_1^*, 0)$. Note also that the value of $\lambda_{1,1}^*$ ($\simeq -1.6$) agrees well with the 1D critical Floquet multiplier λ^* ($= -1.601\cdots$).[1] Consequently, the first drive subsystem comes to be in the usual Feigenbaum critical state.

However, the scaling behavior in the second response subsystem exhibits a new type of non-Feigenbaum scaling behavior, as shown in Table II. As n is increased, the sequence of values of the parameter scaling factor $\delta_{2,n}$ approaches the limit value δ_2 ($\simeq 2.39$), and the sequences of values of the orbital scaling factors $\alpha_{x_2,n}$ and

Table I. Sequences of the critical point, the first critical residue, the parameter and orbital scaling factors, $\{A_n^*\}$, $\{R_{1,n}^*\}$, $\{\delta_{1,n}\}$, $\{\alpha_{x_1,n}\}$, and $\{\alpha_{y_1,n}\}$, in the first subsystem, obtained using the residue-matching RG method.

n	A_n^*	$R_{1,n}^*$	$\delta_{1,n}$	$\alpha_{x_1,n}$	$\alpha_{y_1,n}$
4	1.834 472 170	1.299 61	4.683 13	−1.814	−2.254
5	1.834 473 248	1.300 65	4.668 18	−2.670	−2.565
6	1.834 473 231	1.300 57	4.669 49	−2.443	−2.482
7	1.834 473 235	1.300 65	4.668 91	−2.528	−2.512
8	1.834 473 233	1.300 45	4.668 99	−2.493	−2.500
9	1.834 473 234	1.300 96	4.669 12	−2.506	−2.504

Table II. Sequences of the critical point, the second critical residue, the parameter and orbital scaling factors, $\{B_n^*\}$, $\{R_{2,n}^*\}$, $\{\delta_{2,n}\}$, $\{\alpha_{x_2,n}\}$, and $\{\alpha_{y_2,n}\}$, in the second subsystem, obtained using the residue-matching RG method.

n	B_n^*	$R_{2,n}^*$	$\delta_{2,n}$	$\alpha_{x_2,n}$	$\alpha_{y_2,n}$
4	1.849 576	1.072 1	2.453	−1.14	−1.43
5	1.849 658	1.080 8	2.409	−1.69	−1.56
6	1.849 694	1.089 9	2.406	−1.38	−1.45
7	1.849 689	1.086 4	2.401	−1.58	−1.53
8	1.849 691	1.089 5	2.399	−1.45	−1.48
9	1.849 690	1.088 1	2.391	−1.54	−1.51

$\alpha_{y_2,n}$ converge to the same limit value α_2 ($\simeq -1.5$). Note that these limit values δ_2 and α_2 agree well with the scaling factors δ_2 ($= 2.392\cdots$) and α_2 ($= -1.505\cdots$) in the second response subsystem for unidirectionally-coupled 1D maps.[7),8)] When n is increased, the sequence of the critical residue $\mathcal{R}^*_{2,n}$ also converges to the limit value $\mathcal{R}^*$ ($\simeq 1.09$), and hence the corresponding pair of critical Floquet multipliers $(\lambda^*_{2,1}, \lambda^*_{2,2})$ becomes $(1-2R^*_2, 0)$ [$\simeq (-1.18, 0)$]. Here the value of $\lambda^*_{2,1}$ also agrees well with the second critical Floquet multiplier λ^*_2 ($= -1.178\cdots$) in the second response subsystem for the unidirectionally-coupled 1D maps.[7),8)] Consequently, the bicritical scaling behavior in the unidirectionally coupled DWDOs becomes the same as that in the unidirectionally coupled 1D maps.

To confirm the RG results, we also investigated the bicritical scaling behavior with a direct numerical method. Consider a pair of the parameter values (A_n, B_n), at which the periodic orbit of level n (period 2^n) has the residues $R_{1,n} = R_{2,n} = 1$. Note that the point (A_n, B_n) corresponds to the threshold of instability in both subsystems. Some such points are denoted by open circles in Fig. 2. Then the sequence of values of (A_n, B_n) converges to the lower-left bicritical point (A_c, B_c), denoted by the solid circle, as the level n is increased. To locate this bicritical point with a satisfactory precision, we directly follow the orbits of period 2^n up to level $n = 10$, and obtain the sequences of both the parameters (A_n, B_n) and the orbit points $\boldsymbol{z}_n$ [$= (z_{1,n}, z_{2,n})$] whose distance from its nearest orbit point is maximal, where $z_{i,n} = (x_{i,n}, y_{i,n})$ $(i = 1, 2)$.

The types of asymptotic scaling behavior of the above sequences near the lower-left bicritical point were investigated in both subsystems. Note that the scaling behavior in the first drive subsystem is obviously the same as that in the uncoupled DWDO.[18)] Hence, as in the uncoupled DWDO, the sequences $\{A_n\}$, $\{x_{1,n}\}$, and $\{y_{1,n}\}$ converge to their limit values $A^{\rm F}_\infty$ ($= 1.834\,473\,234$), x^*_1 ($= 0.663\,451\,6$), and y^*_1 ($= 0.990\,119\,2$) geometrically with the 1D asymptotic ratios, respectively:

$$A_n - A^{\rm F}_\infty \sim \delta_1^{-n}, \quad x_{1,n} - x^*_1 \sim \alpha_1^{-n}, \quad y_{1,n} - y^*_1 \sim \alpha_1^{-n}. \tag{21}$$

Here the limit values are obtained using the superconverging method,[23)] and the scaling factors δ_1 and α_1 are just the Feigenbaum constants δ ($= 4.669\cdots$) and α ($= -2.502\cdots$) for the 1D maps, respectively. However, the second response subsystem exhibits non-Feigenbaum scaling behavior. The sequences $\{B_n\}$,$\{x_{2,n}\}$, and $\{y_{2,n}\}$ also converge geometrically to their limit values B_c ($= 1.849\,69$), x^*_2 ($= 0.660\,87$), and y^*_2 ($= 0.989\,91$), where the limit values are also obtained using the superconverging method. To obtain the convergence rates of the sequences, we define the scaling factors of level n as

$$\delta_{2,n} \equiv \frac{B_{n-1} - B_n}{B_n - B_{n+1}}, \quad \alpha_{x_2,n} \equiv \frac{x_{2,n-1} - x_{2,n}}{x_{2,n} - x_{2,n+1}}, \quad \alpha_{y_2,n} \equiv \frac{y_{2,n-1} - y_{2,n}}{y_{2,n} - y_{2,n+1}}. \tag{22}$$

The sequence $\{\delta_{2,n}\}$ is listed in Table III, and it seems to converge to the limit value δ_2 (~ 2.39) obtained using the RG method. Both the sequences $\{\alpha_{x_2,n}\}$ and $\{\alpha_{y_2,n}\}$ also seem to approach the same limit value α_2 ($\simeq -1.5$) obtained using the RG method.

To demonstrate the parameter scaling, we study the "topography" of the parameter plane. Figure 4 displays the phase diagrams near the lower-left bicritical point. States in the parameter plane are determined by calculating their Lyapunov exponents. The white areas correspond to periodic states, and the numbers denote the periods. The vertical and horizontal dashes denote chaotic states in the first and second subsystems, respectively, and crosses correspond to hyperchaotic states with two positive Lyapunov exponents. The pictures in Figs. 4(b) and (c) were obtained by magnifying the regions in the small boxes in the previous pictures by the scaling factor δ_1 for the A axis and δ_2 for the B axis. Note that each successive picture reproduces the previous one with an accuracy that increases with the depth of resolution.

Table III. Sequences of the parameter and orbital scaling factors, $\{\delta_{2,n}\}$, $\{\alpha_{x_2,n}\}$, and $\{\alpha_{y_2,n}\}$, in the second subsystem, obtained by directly following the "self-similar" parameter and orbital sequences.

n	$\delta_{2,n}$	$\alpha_{x_2,n}$	$\alpha_{y_2,n}$
5	1.30	−1.491	−1.691
6	1.34	−1.615	−1.494
7	2.73	−1.495	−1.572
8	2.24	−1.547	−1.497
9	2.56	−1.498	−1.530

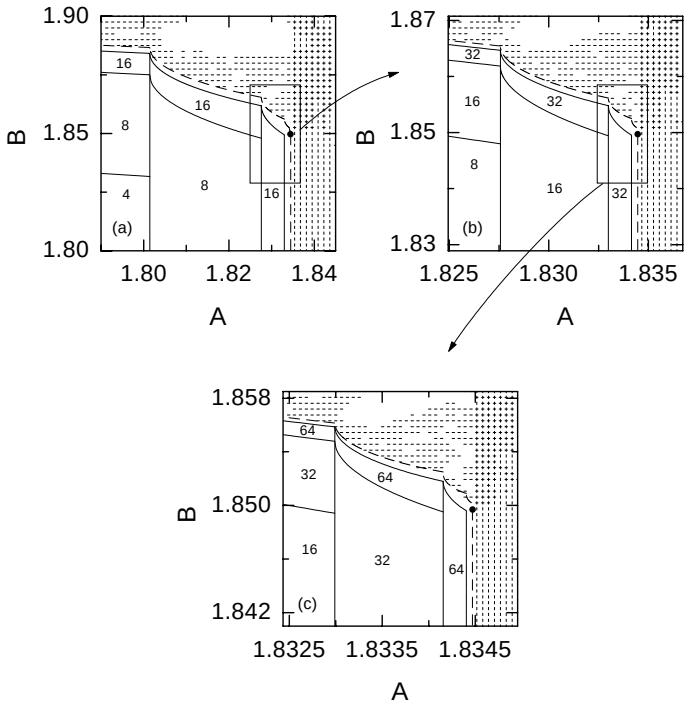

Fig. 4. Phase diagrams near the lower-left bicritical point for $C = -0.1$. States in the parameter plane are determined by their Lyapunov exponents. The white areas correspond to periodic states and the numbers denote the periods. Vertical and horizontal dashes denote chaotic states in the first and second subsystems, respectively, and crosses correspond to hyperchaotic states with two positive Lyapunov exponents. The pictures in (b) and (c) were obtained by magnifying the regions in the small boxes in the previous pictures by the scaling factor δ_1 for the A axis and δ_2 for the B axis. Each successive picture reproduces the previous one with an accuracy increasing with the depth of resolution.

olution. Hence, the configuration of states in Fig. 4 demonstrates the parameter scaling near the bicritical point.

For further evidence of scaling, we also compare the hyperchaotic attractors, shown in Fig. 5, for three values of the pair (A, B) near the lower-left bicritical point (A_c, B_c). Figure 5(a) displays the 2D projection of a hyperchaotic attractor onto the x_1-x_2 plane with the origin shifted at (x_1^*, x_2^*) for $A = A_c^{(1)} + \Delta A$ and $B = B_c^{(1)} + \Delta B$, where $\Delta A = 0.0008$ and $\Delta B = 0.0035$. This hyperchaotic attractor has two positive Lyapunov exponents, $\sigma_{1,1} \simeq 0.021$ and $\sigma_{2,1} \simeq 0.0048$. To observe scaling, we first rescale ΔA and ΔB with the parameter scal-

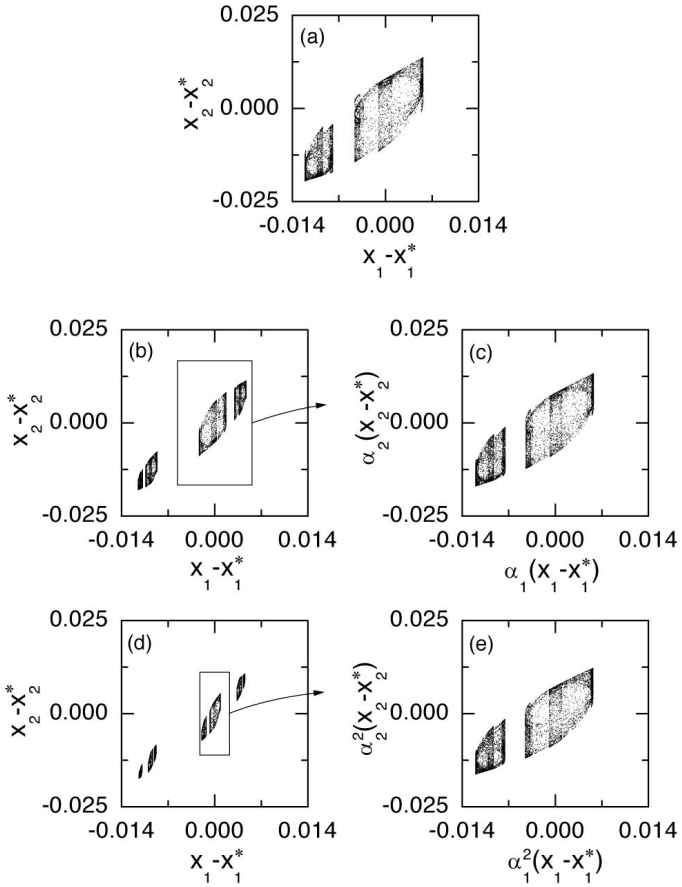

Fig. 5. Hyperchaotic attractors for the three values of (A, B) near the lower-left bicritical point (A_c, B_c) for $C = -0.1$. In (a), $(A, B) = (A_c^{(1)} + \Delta A, B_c^{(1)} + \Delta B)$ ($\Delta A = 0.0008$, $\Delta B = 0.0035$), in (b) and (c), $(A, B) = (A_c^{(1)} + \Delta A/\delta_1, B_c^{(1)} + \Delta B/\delta_2)$, and in (d) and (e), $(A, B) = (A_c^{(1)} + \Delta A/\delta_1^2, B_c^{(1)} + \Delta B/\delta_2^2)$. The picture in (c) is obtained by magnifying the region in the small box in (b) with the scaling factors α_1 for the x_1 axis and α_2 for the x_2 axis. Similarly, we also obtain the picture (e) by magnifying the region inside the small box in (d) with the scaling factors α_1^2 for the x_1 axis and α_2^2 for the x_2 axis. Comparing the pictures in (a), (c), and (e), we can see that each successive magnified picture reproduces the previous one with an accuracy corresponding to the depth of resolution.

ing factors δ_1 and δ_2, respectively. The 2D projection of the attractor for the rescaled parameter values $A = A_c + \Delta A/\delta_1$ and $B = B_c + \Delta B/\delta_2$ is shown in Fig. 5(b). It is also the hyperchaotic attractor with $\sigma_1 \simeq 0.011$ and $\sigma_2 \simeq 0.0024$. We next magnify the region in the small box (containing the origin) by the scaling factor α_1 for the x_1 axis and α_2 for the x_2 axis, thereby obtaining the magnified picture in Fig. 5(c). Note that the picture in Fig. 5(c) reproduces the previous one in Fig. 5(a) approximately. Repeating the above procedure once more, we obtain the two pictures in Figs. 5(d) and (e). That is, Fig. 5(d) displays the hyperchaotic attractor with $\sigma \simeq 0.0063$ and $\sigma_2 \simeq 0.0013$ for $A = A_c + \Delta A/\delta_1^2$ and $B = B_c + \Delta B/\delta_2^2$. Magnifying the region in the small box with the scaling factors α_1^2 for the x_1-axis and α_2^2 for the x_2-axis, we also obtain the magnified picture in Fig. 5(e), which reproduces the previous one in Fig. 5(c) with increased accuracy.

We now turn to a brief discussion of the behavior exactly at the lower-left bicritical point. There exists an infinite number of unstable periodic orbits with period 2^n, forming the skeleton of the bicritical attractor. The orbit points $z_{1,n}$ and $z_{2,n}$ that are maximally distant from their nearest orbit points in the first and second subsystems are found to converge geometrically to their limit points z_1^* and z_2^* with the asymptotic ratios α_1 and α_2. The residues $R_{1,n}$ and $R_{2,n}$ of the orbits with period 2^n are also found to converge to the critical residues R_1^* and R_2^*.

In addition to the above considered case of the lower-left bicritical point, we also study the scaling behavior near the three other bicritical points, the lower-right bicritical point at $(A_\infty^{\mathrm{B}}, 2.025\,63)$, the upper-left bicritical point at $(A_\infty^{\mathrm{F}}, 4.532\,51)$, and the upper-right bicritical point at $(A_\infty^{\mathrm{B}}, 4.233\,32)$.

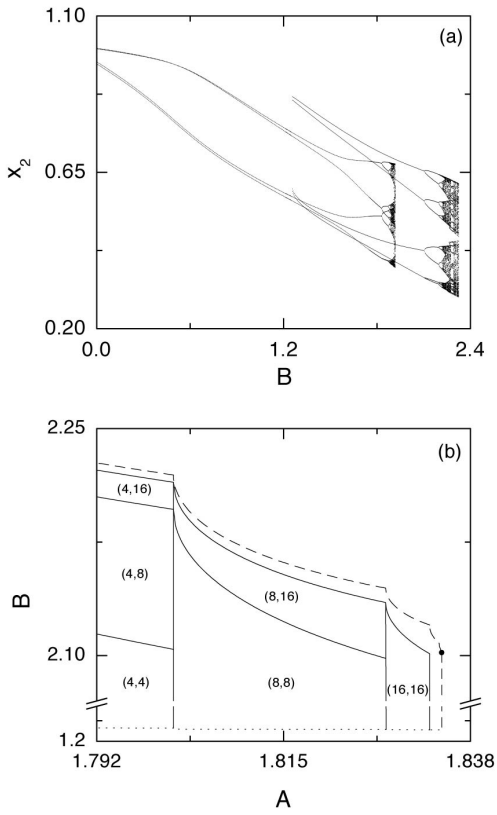

Fig. 6. (a) Two overlapped period-doubling cascades in the second subsystem for $A = 1.8$ and $C = -0.1$. The first cascade starting from $B = 0$ is associated with orbits of type 0_s, while the second one starting from $B = 1.257\,83$ is associated with orbits of type 3_s. (b) Stability diagram of asymmetric orbits of type 3_s for $C = -0.1$. Here each stable region is labelled by the pair of numbers (q_1, q_2), where q_1 and q_2 denote the periods of oscillation in the first and second subsystems, respectively. The lower dotted line represents a saddle-node bifurcation line, at which a period-q attractor of type 3_s is born. The two (vertical and non-vertical) critical lines, denoted by the dashed lines, of period-doubling transitions to chaos meet at the bicritical point, denoted by the solid circle.

The types of scaling behavior near these bicritical points are thus found to be the same as those near the lower-left bicritical point.

To this point, we have studied the bicritical behavior of only in-phase periodic orbits with phase shift $N = 0$. However, as mentioned in §2, there may exist many other types of out-of-phase orbits which appear via saddle-node bifurcations. Note that these out-of-phase orbits exhibit the same types of bicritical scaling behavior. As an example, we consider the case of $A = 1.8$, at which the first drive system is in the period-4 state. A bifurcation diagram for the second response subsystem is shown in Fig. 6(a). As we see, there are two overlapped period-doubling cascades, each of which begins from the period-4 cycle, because it is just the period of the external driving forcing produced by the first subsystem. The orbits in the first period-doubling cascade starting from $B = 0$ are orbits of type 0_s, because they are in-phase (phase shift $N = 0$) and consist of the same pairs when coming to $A = B$ and $C = 0$. The orbits in the second period-doubling cascade beginning from $B = 1.257\,83$, at which an out-of-phase period-4 attractor is born via a saddle-node bifurcation, are orbits of type 3_s because they are out-of-phase with phase shift $N = 3$ and consist of the same pair. Figure 6(b) displays the stability diagram associated with out-of-phase orbits of type 3_s. Note that the structure of this stability diagram is the same as that in the lower-left stability diagram in Fig. 2 for the case of in-phase orbits. The scaling behavior near the bicritical point denoted by the solid circle is also found to be the same as that for the case of in-phase orbits.

To examine the coupling effect on the bicritical behavior, we also consider a system consisting of two DWDOs with a unidirectional coupling of general type, described by

$$\dot{x}_1 = y_1, \tag{23a}$$
$$\dot{y}_1 = f_A(x_1, y_1, t), \tag{23b}$$
$$\dot{x}_2 = y_2 + g_1(x_1, y_1, x_2, y_2), \tag{23c}$$
$$\dot{y}_2 = f_B(x_2, y_2, t) + g_2(x_1, y_1, x_2, y_2), \tag{23d}$$

where $f_A(x, y, t) = -\gamma y + x - x^3 + A\cos\omega t$, and A and B are the control parameters of the two subsystems. For this unidirectionally coupled system, the first DWDO with state variables x_1 and y_1 is a master subsystem driving the second slave or response DWDO with state variables x_2 and y_2 through the generalized coupling terms g_1 and g_2. The bicritical behavior is investigated for the cases of the following six types of couplings:

$$g_1 = C(x_2 - x_1), \quad g_2 = C(y_2 - y_1), \tag{24a}$$
$$g_1 = C(x_2 - x_1), \quad g_2 = 0, \tag{24b}$$
$$g_1 = 0, \quad g_2 = C(y_2 - y_1), \tag{24c}$$
$$g_1 = 0, \quad g_2 = C(x_2 - x_1), \tag{24d}$$
$$g_1 = C(x_2^2 - x_1^2), \quad g_2 = C(y_2^2 - y_1^2), \tag{24e}$$
$$g_1 = C(x_2^3 - x_1^3), \quad g_2 = C(y_2^3 - y_1^3). \tag{24f}$$

Here C is a coupling parameter. The first type of coupling is the coupling considered in Eq. (2d), and all couplings are dissipative, except for that in Eq. (24d). It is thus found that the types of scaling behavior near the bicritical points are the same, irrespective of the type of couplings, although the type of the mother orbits for the period-doubling cascades depends on the type of couplings. That is, the types of bicritical behavior become the same, whether the couplings are dissipative or not. As an example, consider the third type of coupling in Eq. (24c). Figure 7 shows the stability diagram of asymmetric periodic orbits for $C = -0.1$. We first note that the structure of this stability diagram is the same as that in the lower-left stability diagram in Fig. 2 for the first type of coupling. The scaling behavior near the bicritical point denoted by the solid circle is also found to be the same as that for the first type of coupling, although the type of mother orbits is different from that for the first type of coupling. For this case, the type of mother orbits that exist from $B = 0$ is "2_d", because they are out-of-phase orbits with phase-shift $N = 2$ and consist of different pairs when coming to $A = B$ and $C = 0$ (refer to §2 for the types of orbits).

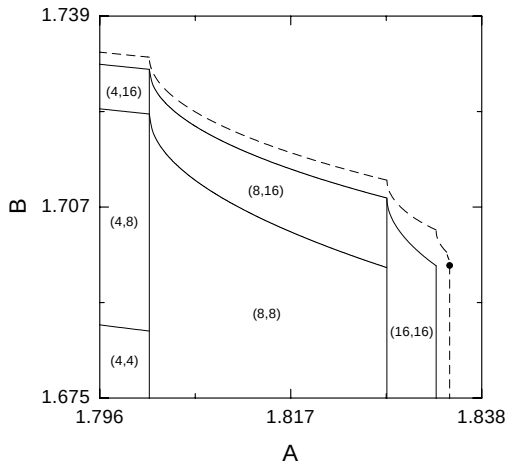

Fig. 7. Stability diagram of asymmetric periodic orbits for the third type of coupling with $g_1 = 0$ and $g_2 = C(y_2 - y_1)$ for $C = -0.1$. Here each stable region is labelled by the pair of numbers (q_1, q_2), where q_1 and q_2 denote the periods of oscillation in the first and second subsystems, respectively. The two (vertical and non-vertical) critical lines, denoted by the dashed lines, of period-doubling transitions to chaos meet at the bicritical point, denoted by the solid circle. Note that the structure of this stability diagram is the same as that of the lower-left stability diagram for the first type of coupling.

To this point, we have fixed the value of the damping parameter to $\gamma = 0.2$. To examine the damping effect on the bicritical behavior, we consider three other cases $\gamma = 0.3$, 0.4, and 0.5. Figure 8 displays the stability diagrams for the orbits of type 0_s that exist from $B = 0$. The structure of these stability diagrams is the same as that in the lower-left stability diagram in Fig. 2 for the case of $\gamma = 0.2$. Note also that the scaling behavior near the bicritical points denoted by solid circles is the same as that for the case of $\gamma = 0.2$, irrespective of the value of γ.

Finally, to examine the universality of the bicriticality we investigate another unidirectionally coupled system consisting of two autonomous Rössler oscillators, described by

$$\dot{x}_1 = y_1 - z_1, \tag{25a}$$

$$\dot{y}_1 = x_1 + a y_1, \tag{25b}$$

$$\dot{z}_1 = b z_1 (x_1 - c_1) \tag{25c}$$

$$\dot{x}_2 = y_2 - z_2 + \epsilon (x_2 - x_1), \tag{25d}$$

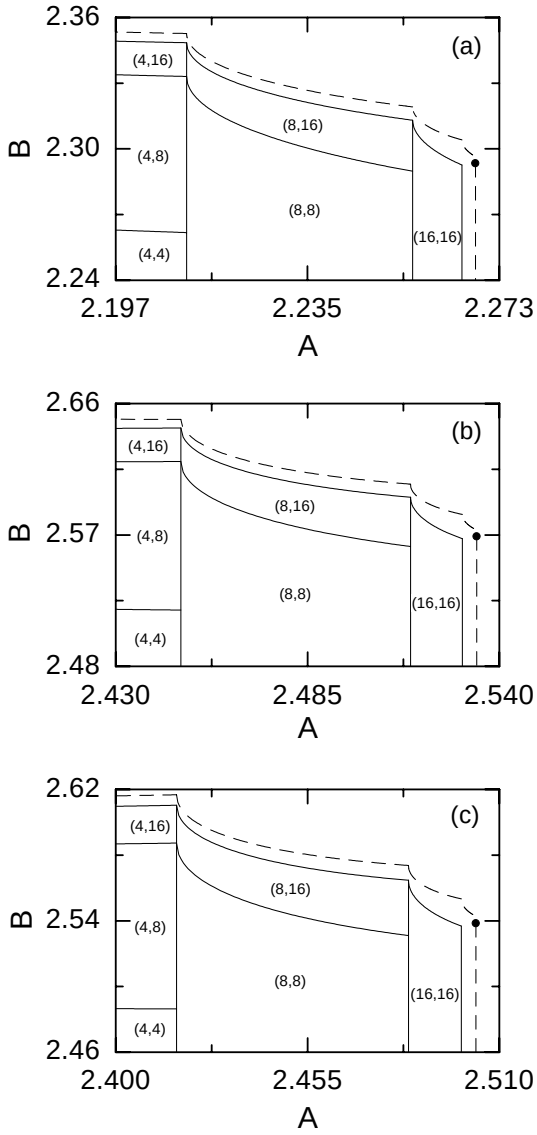

Fig. 8. Stability diagrams of asymmetric orbits of type 0_s for (a) $\gamma = 0.3$ and $\omega = 2.8$, (b) $\gamma = 0.4$ and $\omega = 2.75$, and (c) $\gamma = 0.5$ and $\omega = 2.65$. Here each stable region is labelled by the pair of numbers (q_1, q_2), where q_1 and q_2 denote the periods of oscillation in the first and second subsystems, respectively. The two (vertical and non-vertical) critical lines, denoted by the dashed lines, of period-doubling transitions to chaos in each stability diagram meet at the bicritical point, denoted by the solid circle.

$$\dot{y}_2 = x_2 + a y_2 + \epsilon(y_2 - y_1), \tag{25e}$$

$$\dot{z}_2 = b z_2 (x_2 - c_2) + \epsilon(z_2 - z_1), \tag{25f}$$

where $a = b = 0.2$, c_i $(i = 1, 2)$ is the control parameter of the ith subsystem, and ϵ is the coupling parameter between the two subsystem. For this unidirectionally coupled system, the first Rössler oscillator with state variables x_1, y_1, and z_1 is a

master subsystem driving the second response Rössler oscillator with state variables x_2, y_2, and z_2 through the coupling term. Figure 9 displays the stability diagram for the in-phase orbits when $\epsilon = -0.01$. We first note the "universal" structure of the stability diagram (compare the stability diagram in Fig. 9 with the lower-left stability diagram in Fig. 2). The scaling behavior near the bicritical point denoted by the solid cicle is also found to be the same as that for unidirectionally coupled Duffing oscillators. Consequently, we find that completely different unidirectionally coupled systems exhibit the same universal bicritical behavior.

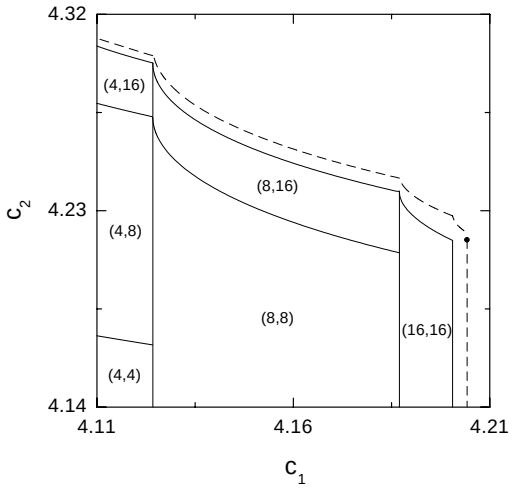

Fig. 9. Stability diagram of in-phase orbits for $\epsilon = -0.01$ for the unidirectionally coupled Rössler oscillators. Here each stable region is labelled by the pair of numbers (q_1, q_2), where q_1 and q_2 denote the periods of oscillation in the first and second subsystems, respectively. The two (vertical and non-vertical) critical lines, denoted by the dashed lines, of period-doubling transitions to chaos in each stability diagram meet at the bicritical point, denoted by the solid circle.

§4. Summary

To confirm the universality of the bicriticality in an abstract system of two unidirectionally coupled 1D maps, we have studied the bicritical scaling behavior of period doublings in two unidirectionally coupled DWDOs. As the control parameters are varied, the first and second subsystems may undergo forward and backward period-doubling cascades, leading to chaos. Then, the critical lines of period-doubling transitions to chaos in the two subsystems meet at four bicritical points. When crossing a bicritical point, corresponding to the threshold of chaos in both subsystems, a transition to hyperchaos occurs (i.e., a hyperchaotic attractor with two Lyapunov exponents appears). Using both the residue-matching RG method and a direct numerical method, we have investigated scaling behavior near the bicritical points, and found a new kind of non-Feigenbaum scaling behavior in the response subsystem. To examine the universality of the bicritical scaling behavior, another unidirectionally coupled system consisting of autonomous Rössler oscillators has also been investigated. Note that the types of bicritical scaling behavior of these unidirectionally coupled oscillators are the same as those in two unidirectionally coupled 1D maps. We thus hypothesize that the bicriticality occurs generally in a large class of unidirectionally coupled systems consisting of period-doubling subsystems.

Acknowledgements

This work was supported by the Interdisciplinary Research Program of the Korea Science and Engineering Foundation under Grant No. 1999-2-112-004-3.

References

1) M. J. Feigenbaum, J. Stat. Phys. **19** (1978), 25; **21** (1979), 669.
2) P. Cvitanović, in *Universality in chaos*, ed. P. Cvitanović (Adam Hilger, Bristol, 1984), p. 3.
3) S. P. Kuznetsov, Radiophys. Quantum Electron. **28** (1985), 681.
   S. P. Kuznetsov and A. S. Pikovsky, Physica **D19** (1986), 384.
4) S.-Y. Kim and H. Kook, Phys. Rev. **A46** (1992), R4467; Phys. Lett. **A178** (1993), 258; Phys. Rev. **E48** (1993), 785.
   S.-Y. Kim, Phys. Rev. **E54** (1996), 3393.
5) S.-Y. Kim and K. Lee, Phys. Rev. **E54** (1996), 1237.
   S.-Y. Kim and B. Hu, Phys. Rev. **E58** (1998), 7231.
6) I. Waller and R. Kapral, Phys. Rev. **A30** (1984), 2047.
   H. Kook, F. H. Ling and G. Schmidt, Phys. Rev. **A43** (1991), 2700.
7) A. P. Kuznetsov, S. P. Kuznetsov and I. R. Sataev, Int. J. Bifurcation and Chaos Appl. Sci. Eng. **1** (1991), 839; Physica **D109** (1997), 91.
8) S.-Y. Kim, Phys. Rev. **E59** (1999), 6585.
9) B. P. Bezruchko, V. Yu. Gulyaev, S. P. Kuznetsov and E. P. Seleznev, Dokl. Akad. Nauk SSSR **287** (1986), 619 [Sov. Phys. -Dokl. **31** (1986), 268].
   A. P. Kuznetsov, S. P. Kuznetsov and I. R. Saraev, Int. J. Bifurcation and Chaos Appl. Sci. Eng. **6** (1996), 119.
10) K. Kaneko, Phys. Lett. **A111** (1985), 321.
    I. S. Aranson, A. V. Gaponov-Grekhov and M. I. Rabinovich, Physica **D33** (1988), 1.
    F. H. Willeboordse and K. Kaneko, Phys. Rev. Lett. **73** (1994), 533; Physica **D86** (1995), 428.
    O. Rudzick and A. Pikovsky, Phys. Rev. **E54** (1996), 5107.
11) P. J. Holmes, Philos. Trans. R. Soc. London Ser. **A292** (1979), 419.
    F. C. Moon and P. J. Holmes, J. Sound Vib. **65** (1979), 275.
    R. A. Mahaffey, Phys. Fluid **19** (1976), 1387.
    F. C. Moon and G.-X. Li, Phys. Rev. Lett. **55** (1985), 1439.
    F. T. Arecchi and F. Lisi, Phys. Rev. Lett. **49** (1982), 94.
    H. Ishii, H. Fujisaka and M. Inoue, Phys. Lett. **A116** (1986), 257.
    S.-Y. Kim and Y. Kim, Phys. Rev. **E61** (2000), 6517.
    Y. Kim, S. Y. Lee and S.-Y. Kim, Phys. Lett. **A275** (2000), 254.
12) K. M. Campbell and M. E. Davies, Nonlinearity **9** (1996), 801.
    K. M. Campbell, Physica **D107** (1997), 43.
13) T. C. Newell, V. Kovanis and A. Gavrielides, Phys. Rev. Lett. **77** (1996), 1747 and references therein.
14) O. E. Rössler, Phys. Lett. **A71** (1979), 155.
    K. Kaneko, Prog. Theor. Phys. **69** (1983), 1427.
    T. Kapitaniak and W.-H. Steeb, Phys. Lett. **A152** (1991), 33.
    M. C. de Sousa Vieira, A. J. Lichtenberg and M. A. Lieberman, Phys. Rev. **A46** (1992), R7359.
    T. Kapitaniak and L. O. Chua, Int. J. Bifurcation and Chaos Appl. Sci. Eng. **4** (1994), 477.
    M. A. Harrison and Y.-C. Lai, Phys. Rev. **E59** (1999), R3799.
15) O. E. Rössler, Phys. Rev. **A57** (1976), 397.
16) S.-Y. Kim and B. Hu, Phys. Rev. **A44** (1991), 934.
    S.-Y. Kim and D.-S. Lee, Phys. Rev. **A45** (1992), 5480.
17) S. Lefschetz, *Differential Equations: Geometric Theory* (Dover Publications, Inc., New York, 1977), Sec. 3.5.
18) S.-Y. Kim, Int. J. Mod. Phys. **B14** (2000), 1801.
19) V. I. Arnold, *Ordinary Differential Equations* (MIT Press, Cambridge, 1973), p. 114.
20) J. M. Greene, J. Math. Phys. **20** (1979), 1183.
    R. S. MacKay, Physica **D7** (1983), 283.
21) J. Guckenheimer and P. Holmes, *Nonlinear Oscillations, Dynamical Systems and Bifurcations of Vector Fields* (Springer-Verlag, New York, 1983), Sec. 3.5.
22) A. J. Lichtenberg and M. A. Lieberman, *Regular and Stochastic Motion* (Springer-Verlag, New York, 1983), Sec. 5.3.

23) R. S. MacKay, Ph.D. thesis, Princeton University, 1982. See Eqs. 3.1.2.12 and 3.1.2.13.